

Efficient Frequency Allocation for Superconducting Quantum Processors Using Improved Optimization Techniques

Zewen Zhang,^{1,2} Pranav Gokhale,³ and Jeffrey M. Larson¹

¹*Mathematics and Computer Science Division, Argonne National Laboratory, Lemont, Illinois 60439, USA*

²*Department of Physics and Astronomy, Rice University, Houston, Texas 77005, USA*

³*Infleqtion, Chicago, Illinois 60604, USA*

(Dated: October 29, 2024)

Building on previous research on frequency allocation optimization for superconducting circuit quantum processors, this work incorporates several new techniques to improve overall solution quality. New features include tightening constraints, imposing edgewise differences, including edge orientation in the optimization, and integrating multimodule designs with various boundary conditions. These enhancements allow for greater flexibility in processor design by eliminating the need for handpicked orientations. We support the efficient assembly of large processors with dense connectivity by choosing the best boundary conditions. Examples demonstrate that, at low computational cost, the new optimization approach finds a frequency configuration for a square chip with over 1,000 qubits and over 10% yield at much larger dispersion levels than required by previous approaches.

I. INTRODUCTION

Superconducting (SC) quantum processors have led to significant progress in numerous domains, including demonstrations of quantum advantage [1, 2], quantum error correction [3, 4], variational methods [5–8], and analog simulations [9, 10]. Among competing quantum architectures, fixed-frequency SC devices are a leading technology due to their high coherence, relatively simple control, and ability to scale up to hundreds of qubits in state-of-the-art devices [2, 11]. However, the need for addressability, which requires large detunings among neighboring qubits, and controllability, which is set by the entangling protocol, imposes constraints on selecting local frequencies for each qubit [12–14]; these constraints present challenges in SC chip manufacturing and hinder the scalability and connectivity of these devices. Therefore, solving frequency allocation problems is critical to the success of fixed-frequency SC devices.

Moreover, recent developments in quantum error correction have further increased the potential for frequency crowding, heightening the need for improved techniques for avoiding frequency collision. In particular, while the nearest-neighbor surface code [15] quantum error correction architecture has historically been favored for SC processors, advances in the study of non-local qLDPC codes [16, 17] have placed them at the forefront of emerging roadmaps. We highlight two examples here. One recent work by IBM [18] has discovered distance-12 qLDPC codes that encode 12 logical qubits into 144 physical qubits—this is over 10 times more space-efficient than the equivalent surface code. However, this code requires degree-6 qubit connectivity, substantially increasing the frequency collision risk over degree-4 surface code interaction graphs. While the frequency collision overhead could be mitigated by switching to an SC device with tunable couplers and/or frequency-tunable qubits, doing so would add significant complexity to control and wiring

requirements. In a similar spirit, another recent work [19] demonstrates that IBM’s code could be remapped to a single plane that permits two-qubit gates across qubits up to 7.22 units away, that is, (6,4) units away in taxicab geometry. While this approach is favored from the perspective of having shorter long-range connections, it would lead to even greater chances of frequency collisions because of the relative geometric locality of the frequency crowding. Thus, while non-local qLDPC codes offer a promising path forward for more efficient quantum error correction, they also amplify challenges associated with frequency collisions.

Another prevailing trend that induces even greater conditions on frequency requirements is an increased interest in qutrit and qudit systems in quantum applications. As a baseline, many two-qubit gates in SC systems in fact use qutrit states to perform entangling operations. In addition, IBM now routinely performs qubit readout via excited state promotion, a technique that excites $|1\rangle$ to $|2\rangle$ prior to measurement [20]. Moreover, algorithmic research [21] has demonstrated that computing with qutrits can achieve an exponential advantage in runtime over qubits. Because of these developments, quantum hardware designers are motivated to support qudit control [22]; however, this shift further increases the risk of frequency collisions, as additional relevant frequencies (e.g., $|1\rangle \rightarrow |2\rangle$) must also be avoided.

When designing an SC device, the individual frequency f_i of each qubit i is determined by the critical current of the Josephson junction and the circuit’s capacitance. As with any manufacturing process, frequencies are often fabricated with a certain degree of uncertainty, which can lead to constraint violations between neighboring qubits (“frequency collision”) and, consequently, reduce the success ratio of producing collision-free processors (“yield”) during manufacturing. Various optimization methods have been implemented to address frequency allocation in SC devices, aiming to reduce the probability of frequency collisions and improve yield when manufacturing

chips, while balancing computational resources required for optimization strategies. Even with novel optimization methods, scaling SC quantum processors with desired connectivity to hundreds of qubits is challenging and often results in an exponentially low yield. Significant progress in solving frequency allocation problems has been made using numerical tools such as mixed-integer-programming-based optimization [13], multichip module approaches [23], physics-inspired frameworks [24], Floquet analysis [25], and connectivity optimization [26, 27]. Improvements in SC qubit fabrication have also helped mitigate frequency collisions [28–30]. Optimization challenges persist, however, hindering the production of ideal (large) devices with good connectivity, such as the native devices required for square grid structures for the surface code [15] or the degree-6 connectivity needed for advanced codes [18].

In this work we develop several optimization techniques that build on the mixed-integer-programming-based approach in Ref. [13] to significantly improve device yield compared with previous methods. First, by tightening certain constraints in specific allocation problems, we achieve substantial yield improvements. Second, we address the often overlooked issue of qubit orientation (i.e., determining control and target qubits for each edge) and introduce it as a decision in the optimization process. We also consider adding edgewise differences to our optimization model to avoid some special symmetric solutions allowed by the topology and the objective function, which often lead to low yield in practice. Third, we enhance multichip module design [23] by incorporating various boundary conditions in assembling small modules, allowing the methods to scale to larger problems. With these improved optimization techniques, we can compute frequency configurations for 32×32 square grid chips with over 10% yield at a threshold dispersion of 6.5 MHz, which is around 30% better than the previous results [13].

We now give an outline of the paper. Section II discusses three significant optimization approaches for improving the solution quality to the frequency allocation problem. Section III presents results for how these approaches improve solution quality. Section IV concludes with an outlook on future approaches for addressing frequency allocation problems.

II. FREQUENCY ALLOCATION AND OPTIMIZATION FORMULATION

The fabrication process of SC qubits introduces a stochastic frequency dispersion σ to the value of each desired f_i , which can result in unwanted crosstalk [24]. This dispersion, primarily arising during the fabrication of Josephson junctions [31, 32], maintains a value of around 10 MHz even in the simplest SC qubit structure, the transmon platforms [29, 33]. If exact frequencies could be fabricated (i.e., if σ was zero), the frequency allocation

problem would be greatly simplified. Here we use numerical optimization to determine frequencies f_i that account for this dispersion. Frequency collisions can arise for a variety of physical reasons, each of which can be modeled as a constraint in our numerical optimization model. We consider the same collisions studied in Refs. [13, 33]; their corresponding constraints are listed for completeness in Table I. There are nine families of constraints for SC processors with cross-resonance [34] (CR) entangling gates, which can be sorted in three categories: Addressability (**A1** and **A2**), Entanglement (**C1**, **D1**, **E1**, and **E2**), and Spectator (**S1**, **S2**, and **T1**) constraints [12].

A frequency allocation problem is commonly modeled as occurring on a graph. In this graph the set of vertices (V) represent qubits, and the set of edges (E) represent entangling gates connecting two qubits. A real value f_i is assigned to vertex v_i in V to represent the desired frequency for the i th qubit. Within the CR protocol, orientations must be chosen with specific *control* qubit \rightarrow *target* qubit directions. In the notation, besides the undirected edge set E , the directed edge set is denoted \vec{E} , with $(i, j) \in \vec{E}$, which indicates qubit i is the *control* qubit and qubit j is the *target* qubit. This notation is specifically associated with the entanglement constraints outlined in Table I. In Section II B and beyond, however, as the orientation becomes subject to optimization, no constraints are imposed based on the initial input orientation.

Type	Definition	Participants	Bounds
A1	$ f_i - f_j \geq \delta_{A1}$	$(i, j) \in E$	17 MHz
A2	$ f_i - f_j - \alpha \geq \delta_{A2}$	$(i, j) \in E$	30 MHz
C1	$f_i + \alpha \leq f_d \leq f_i$	$(i, j) \in \vec{E}$	—
E1	$ f_d - f_i \geq \delta_{E1}$	$(i, j) \in \vec{E}$	17 MHz
E2	$ f_d - f_i - \alpha \geq \delta_{E2}$	$(i, j) \in \vec{E}$	30 MHz
D1	$ f_d - f_i - \alpha/2 \geq \delta_{D1}$	$(i, j) \in \vec{E}$	2 MHz
S1	$ f_d - f_k \geq \delta_{S1}$	$(i, j, k) \in N$	17 MHz
S2	$ f_d - f_k - \alpha \geq \delta_{S2}$	$(i, j, k) \in N$	25 MHz
T1	$ f_d + f_k - 2f_i - \alpha \geq \delta_{T1}$	$(i, j, k) \in N$	17 MHz

TABLE I. Original constraints for directed graphs, cited from Ref. [13]. $(i, j, k) \in N$ when $(i, j) \in \vec{E}$ and $(j, k) \in E$. $\alpha = -0.35$ GHz is the anharmonicity of qubits. In the CR protocol, for connected qubit pair $i \rightarrow j$, the driving frequency f_d on the control qubit i is equal to the frequency f_j of the target qubit j [34].

To ensure that the chosen qubit frequencies do not incur collisions, we introduce a variable δ_n for each of the nine types of constraints (for example, δ_{A1} for the **A1** constraints $|f_i - f_j| \geq \delta_{A1}$). Merely setting an objective to maximize $\sum_n \delta_n$ could result in several values of δ_n being large (meaning those types of collisions are unlikely to happen), but other values of δ_n may be zero (meaning collisions of that type are likely to occur with finite dispersion). Instead, we set lower bounds $\bar{\delta}_n$ for each of the δ_n and then set our objective to be maximize $\sum_n (\delta_n - \bar{\delta}_n)$. The values for each $\bar{\delta}_n$ are given in Table I.

Ultimately, we model the frequency allocation problem

as a mixed-integer programming problem; we have made our models freely available¹. We hope that these open-source models support the frequency allocation process in SC devices and inspire other researchers to contribute to their optimization. The numerical results presented below utilize these model with CPLEX as the optimization solver.

As we show, the adverse effects of dispersion can be mitigated through proper optimization strategies. These strategies improve the yield in the fabrication process. [Section II A](#) introduces our tightened constraints and edgewise-difference constraints; [Section II B](#) introduces the orientation of edges as optimization parameters; and [Section II C](#) explains how we can assemble smaller chips into larger chips with various boundary conditions.

A. Constraint Tightening and Edgewise Differences

For a specific topology (i.e., set of edges E), we often observe that frequency collisions are more likely to occur for certain types of constraints. Since the lower bounds of these constraints are set by the fidelity requirement [35], the lower bounds on these types of constraints can be increased for better results. By tightening some constraints—increasing the relevant δ_n values before the optimization process—the yield can be significantly enhanced, as we will demonstrate in [Section III A](#). However, excessively increasing δ_n causes other types of frequency collisions, especially when modeling devices with many qubits. From the optimization perspective, appropriately tightening constraints, especially to account for fabrication dispersion, can considerably improve the yield. Therefore, in practice, it is advisable either to identify the constraints that are more frequently violated for a given problem and impose stricter bounds on those or, more broadly, to tighten all constraints by a tolerance ϵ_{tol} , typically set as a multiple of σ , in order to prevent collisions that might arise from selectively tightening only certain constraints.

As with any mathematical model of a physical system, a disconnect can exist between the predicted and actual effect of selecting a set of frequencies. A higher value of the model objective does not necessarily ensure a higher yield at certain dispersion levels, as shown in [Figure 1](#). In the figure, yields and objective values of optimized solutions are compared for different fixed orientations. For both square and hexagon grids, 10 randomly picked orientations are preset before optimization for comparison. We find that much of the disconnect between the model objective and the yield occurs because some solutions have multiple edges that are exactly at their constraint lower bounds $\bar{\delta}_n$. For example, consider the optimal solution on a 4×4 grid. Previous optimization methods tend

to provide a near-symmetric solution along one of the diagonals, in which most of the edges on the boundary are stuck at the lower bound of constraint **A1** and eventually give low yields. Merely selecting/requiring that f_i differ for each vertex in V can still result in a value of $\|f_i - f_j\|$ that is close to or identical for edges $(i, j) \in E$.

Such duplication of edge differences may be inevitable for some optimization models and can be especially problematic when topologies contain multiple symmetries. In [Figure 1](#) we can see that for given topologies, the orientation that maximizes the model objective does not provide the highest yield at a dispersion of 10 MHz. To address this situation, we impose constraints to ensure there are differences between the frequencies along the edges in the solution. For any two edges k and l with no common qubits shared in the graph, given f_{k1} and f_{k2} (f_{l1} and f_{l2}) as the frequencies of the two qubits attached to edge k (l), we impose

$$\|f_{k1} - f_{k2}\| - \|f_{l1} - f_{l2}\| < \delta_{\text{diff}}, \quad (1)$$

where δ_{diff} is chosen as a small value (empirically $1 \sim 5$ MHz). This rules out solutions where multiple edges are stuck at the lower bound of a specific constraint. For example, following the imposition of [Equation \(1\)](#), an optimized solution will not contain more than one edge positioned at the lower bound of **A1** or on the left side of **C1**. For two edges sharing a qubit, their difference is handled by the spectator constraint **S1** in [Table I](#).

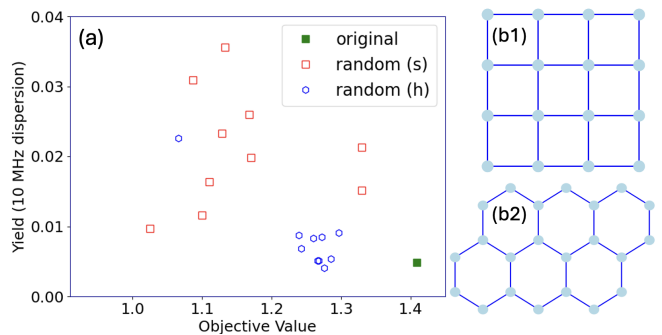


FIG. 1. Yield at dispersion of 10 MHz for different orientations. (a) The optimized objective and yield for 4×4 square (s) grid (b1) and 6-ring hexagon (h) grid (b2). Green solid box: 4×4 square grid using the orientation in Ref. [13]; red open box: 4×4 square grid using random orientations; blue open hexagon: 6-ring hexagon grid using random orientations.

B. Optimization of Edge Orientation

Naturally, the optimized frequency configuration and especially the resulting yield can depend significantly on the chosen orientation of control and target qubits. The choice of orientation is rarely discussed in earlier research. But as we observe in [Figure 1](#), the default orientation [see [Figure 3\(b1\)](#)] for the square grid in some earlier work is not the best.

¹ source code: https://github.com/AlvinZewen/SC_Freq_Allo

A better approach (in our opinion) would be to incorporate orientation into the optimization process: we introduce a set of binary variables $o(i, j)$, where $(i, j) \in E$ labels two qubits connected by an edge. A value of $o(i, j) = 0$ indicates *control* qubit $i \rightarrow$ *target* qubit j , while $o(i, j) = 1$ indicates *control* qubit $j \rightarrow$ *target* qubit i . These binary variables must appear in most directed constraints in the original setting (see Table I), including **C1**, **E1**, **E2**, **D1**, **S1**, **S1**, and **T1**.

As an example, the previous constraint **E2**: $|f_{d,i \rightarrow j} - f_i - \alpha| \geq \delta_{E2}$ depends on the choice of *control* qubit \rightarrow *target* qubit orientation. With the introduction of a sufficiently large positive number M , the **E2** constraint can be written as two constraints that allow for the orientation $o(i, j)$ to be selected by the optimization method:

$$\begin{aligned} |f_j - f_i - \alpha| + M \cdot o(i, j) &\geq \delta_{E2} \\ |f_i - f_j - \alpha| + M \cdot [1 - o(i, j)] &\geq \delta_{E2}. \end{aligned}$$

Similarly, the orientation can be incorporated into other constraints, as shown in Table II. Consequently, only an undirected graph needs to be provided for optimization, with orientation optimized during the process.

C. Multichip Design: Periodic Boundary Condition

In designing larger quantum processors, multichip designs are commonly employed, but the impact of boundary conditions in such designs has seldom been discussed. Analogous to applications in statistical mechanics, boundary conditions can play a crucial role when scaling from small systems to larger ones. Earlier research [13, 23] often assumed periodic boundary conditions, which may not be optimal for SC architecture design.

In this study we tested various boundary conditions for multichip designs, including twisted and Möbius boundary conditions, as shown in Figure 2. Our results emphasize the importance of boundary conditions in assembling multiple small chips into a larger processor. Specifically, for assembling small square chips, our findings identify more effective boundary conditions that generate higher yields than those previously reported.

III. RESULTS: IMPROVED OPTIMIZATION TECHNIQUE

We now present the effects of incorporating the new modeling approaches in Section II. We find that these approaches improve the solution to the frequency allocation problems; as a result, they help find high-yield frequency configurations for large SC processors.

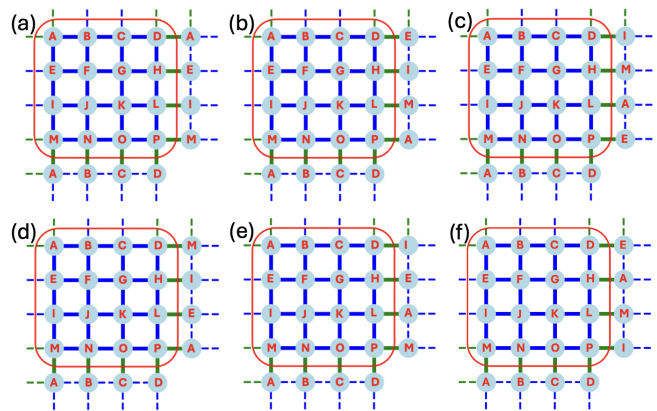


FIG. 2. Tested boundary conditions: (a) conventional periodic boundary condition (PBC1); (b) and (c): twisted boundary conditions (PBC2 and PBC3); (d) Möbius boundary condition (MBC1); (e) and (f): twisted Möbius boundary condition (MBC2 and MBC3).

A. Tightening Constraints

For a specific edge set E with fixed edge orientations, some constraints can be more likely violated than the rest. The occurrence of these types of collisions is substantially reduced when the corresponding constraints are tightened—that is, increasing the $\bar{\delta}_n$ values before optimization. As the examples in Figure 3 show, properly adding tolerance to the constraints leads to significantly higher yields. With (b1) orientation in Figure 3, frequency collisions are likely to occur on **A1** and **S1**; with (b2) orientation, frequency collisions are more probable on **A2** and **S1**. To demonstrate the improvement from constraint tightening, we added tolerance to the **A1** and **S1** constraints for orientation (b1), and the **A2** and **S1** constraints for orientation (b2). As shown in Figure 3, by appropriately setting these tolerance values, the yield can exceed 90%. However, we observed that the yield does not increase monotonically with tolerance. If the tolerance for some constraints is too large, it can induce collisions with other constraints. When the yield drops, conflicts on **A2**, **D1**, and **S2** show up in orientation (b1), and conflicts on **A1** show up in orientation (b2). In the worst-case scenario, excessively increasing certain constraint tolerances can eliminate the possibility of finding any feasible solutions.

These examples suggest maintaining a level of tightened constraints during optimization. Throughout our work we add a tolerance of $\epsilon_{\text{tol}} = 10\text{-}20$ MHz to all constraints except for **D1**. The tolerance for **D1** is omitted for two reasons: first, this constraint is rarely violated in practice; and second, empirically, tightening this constraint sharply slows down the optimization to find a feasible solution and eventually leads to a low-yield solution.

Type	Definition $o(i, j) = 0$		Definition $o(i, j) = 1$		Bounds
C1	$f_i + \alpha \leq f_{d,i \rightarrow j} \leq f_i,$	$(i, j) \in E$	$f_j + \alpha \leq f_{d,j \rightarrow i} \leq f_j,$	$(i, j) \in E$	—
E1	$ f_{d,i \rightarrow j} - f_i \geq \delta_{E1},$	$(i, j) \in E$	$ f_{d,j \rightarrow i} - f_j \geq \delta_{E1},$	$(i, j) \in E$	17 MHz
E2	$ f_{d,i \rightarrow j} - f_i - \alpha \geq \delta_{E2},$	$(i, j) \in E$	$ f_{d,j \rightarrow i} - f_j - \alpha \geq \delta_{E2},$	$(i, j) \in E$	30 MHz
D1	$ f_{d,i \rightarrow j} - f_i - \alpha/2 \geq \delta_{D1},$	$(i, j) \in E$	$ f_{d,j \rightarrow i} - f_j - \alpha/2 \geq \delta_{D1},$	$(i, j) \in E$	2 MHz
S1	$ f_{d,i \rightarrow j} - f_k \geq \delta_{S1}$	$(i, j, k) \in N$	$ f_{d,j \rightarrow i} - f_k \geq \delta_{S1}$	$(j, i, k) \in N$	17 MHz
S2	$ f_{d,i \rightarrow j} - f_k - \alpha \geq \delta_{S2},$	$(i, j, k) \in N$	$ f_{d,j \rightarrow i} - f_k - \alpha \geq \delta_{S2},$	$(j, i, k) \in N$	25 MHz
T1	$ f_{d,i \rightarrow j} + f_k - 2f_i - \alpha \geq \delta_{T1},$	$(i, j, k) \in N$	$ f_{d,j \rightarrow i} + f_k - 2f_j - \alpha \geq \delta_{T1},$	$(j, i, k) \in N$	17 MHz

TABLE II. Modified constraints for undirected graph, with $o(i, j) = 0$ marks $i \rightarrow j$ and $o(i, j) = 1$ marks $i \leftarrow j$. The original constraints of addressability (**A1** and **A2**) are kept.

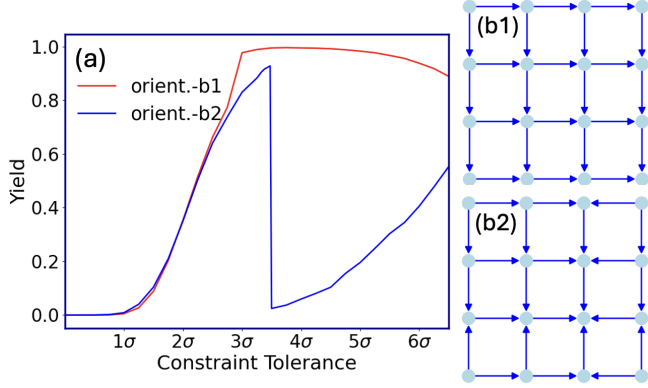


FIG. 3. (a) Yield at dispersion level of $\sigma=10$ MHz for two sets of orientation, with constraint tolerance added in unit of σ , as discussed in the text. (b1) and (b2): Preset orientations of the 4×4 grid. The sudden drop in yield observed in the (b2) curves is caused by the emergence of a different type of constraint violation during frequency reoptimization, as discussed in the main text.

B. Graph Orientation

We now highlight how incorporating the edge orientation within the optimization process can significantly improve yield. In Figure 4(a), when optimized with constraint tolerance $\epsilon_{\text{tol}} = 10$ MHz, the original orientation used in previous research produces the lowest yield. Optimizing on the 10 random orientations as in Figure 1 (at the same tolerance level), all give higher yields than the original orientation does. At 10 MHz dispersion, for both grid and hexagon topologies, with the same constraint tolerance, optimizing the orientation results in over an order of magnitude increase in yield compared with most randomly selected orientation sets. With greater constraint tolerance, as shown by the dashed lines in Figure 4, the yield increases further.

C. Local Yield for Different Boundary Conditions

In assembling small modules into a large chiplet, optimized results significantly depend on boundary conditions. As an example, the frequencies of a 4×4 square grid chip are optimized with the boundary conditions

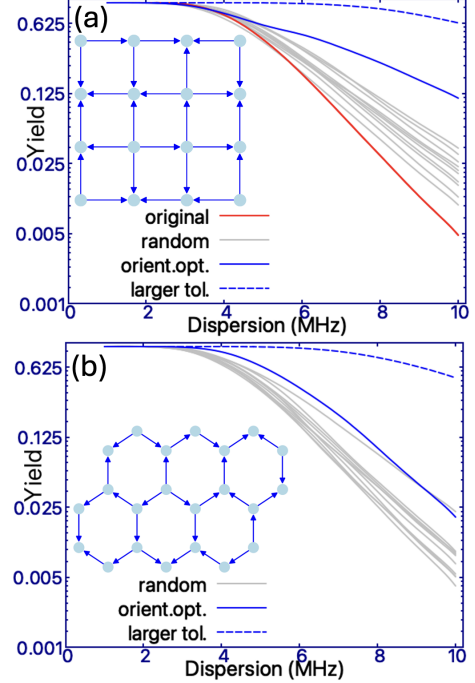


FIG. 4. (a) Yield at different levels of dispersion for different sets of orientation. Red: the orientation used in Ref. [13]; grey: results from 10 random sets of orientation; blue solid: result with orientation optimization and enforced edge differences (as in Equation (1)). (b) Grey: results from 10 random sets of orientation; blue solid: result with orientation optimization and enforced edge differences. In both graphs, the insets give the optimized orientation. All solid curves are optimized with constraint tolerance of 10 MHz, while the dashed curves indicate results with orientation optimization, edge differences imposed and larger constraint tolerance (20 MHz).

presented in Figure 2 and a constraint tolerance $\epsilon_{\text{tol}} = 20$ MHz; the results are shown in Figure 5(a). With the new optimization method and various boundary conditions, we achieve optimized frequency configurations that outperform those in Ref. [13], which requires a frequency dispersion of no larger than 5 MHz to achieve 10% yield for a 1,000-qubit square grid chip. When the local yield of the 4×4 module exceeds 96.5%, combining 62 replicas of these small modules is likely to result in a yield of over 10%. Among all tested boundary conditions, one of the twisted periodic boundary conditions, PBC3, gives the

best performance.

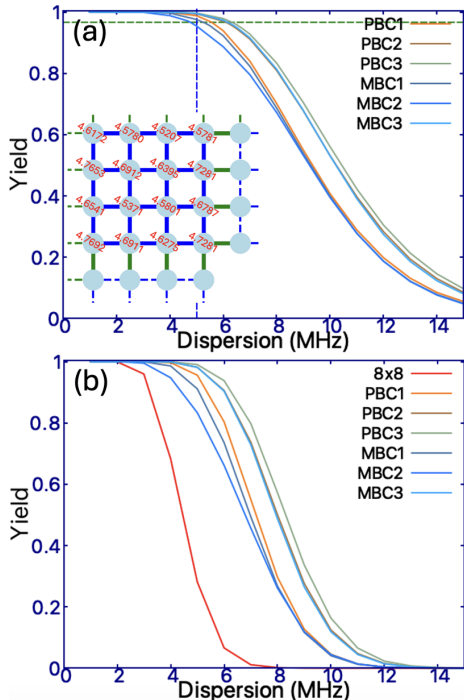


FIG. 5. (a) Performance of local 4×4 modules: the local yield at different levels of dispersion for different sets of periodic boundary conditions. Green line: effective yield of 96.5%; Blue line: dispersion of 5 MHz. Inset: optimal frequency configuration for the best boundary condition [PBC3 in Figure 2]. (b) Assembling a 8×8 chip: red: directly optimizing a 8×8 chip; others: assembling 4×4 chips to a 8×8 chip.

D. Realizing Larger Chips

Multimodule design not only reduces the optimization cost of finding frequency configurations of large chips but also enhances yield under finite computing resources, provided appropriate boundary conditions are applied. Figure 5(b) gives an example of assembling four small modules (4×4 square grids) into one large module (8×8 square grid). These results are compared with the result of directly optimizing an 8×8 chip². The results give clear evidence that the multimodule design outperforms the monochip design in fixed computing resources.

The results also outperform results of the previous optimization method when composing a chip with over 1,000 qubits in square grid topology. The maximum fabrication frequency variation required for a frequency configuration to achieve a 10% yield is referred to here as the

² The multimodule designs are given 20,000 CPU-seconds to optimize with edgewise difference $\delta_{\text{diff}} = 2$ MHz imposed, while directly optimizing the 8×8 chip is given 80,000 seconds, with edgewise difference of $\delta_{\text{diff}} = 0.5$ MHz imposed.

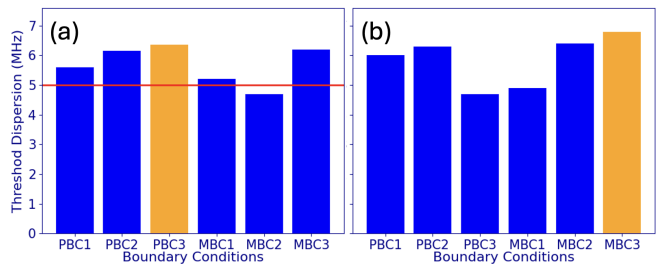


FIG. 6. **Multimodule assembly to 1,000 qubits.** (a) Threshold tolerance on the dispersion of the frequency to achieve 10% yield for a 32×32 square chiplet on different boundary conditions. Red line: dispersion of 5 MHz, which is the best from previous research [13]. Orange bin: the best boundary condition with the same constraint tolerance applied. (b) Threshold tolerance on the dispersion of the frequency to achieve a 10% yield for a 28×35 hexagon chiplet on different boundary conditions.

“threshold frequency.” When assembling 64 small modules together into a 32×32 chiplet, 5 out of 6 tested boundary conditions give a threshold dispersion larger than that given in Ref. [13]. We can also see that, after optimization, some constraints are more likely to experience collisions. As an example, for the PBC3 boundary condition, the three most violated constraints are **A1**, **D1**, and **F1**. Further tightening these constraints can give better results. As the optimal result we can find, the threshold dispersion can go up to around 6.5 MHz, which is a significant improvement from previous research. From the same method, the hexagon grid is tested in a unit cell of 4×5 with different boundary conditions³; the results are shown in Figure 6(b). The best result gives a threshold dispersion of around 7 MHz to make a 28×35 hexagon chiplet, which is comparable to the previous research.

IV. OUTLOOK

We present several improved optimization techniques to address frequency allocation problems in SC circuit processors. These techniques include tightening constraints, imposing edgewise differences, optimizing graph orientations, and incorporating multimodule designs with various boundary conditions. The results highlight the importance and efficiency of these methods.

Specifically, the results demonstrate an increase in the dispersion threshold from 5 MHz to approximately 6.5 MHz for manufacturing square grid processors with over 1,000 qubits. While this threshold still falls short of current transmon technology capabilities, our findings suggest that the potential of optimization methods for frequency allocation is yet to be fully exploited. On the

³ given 80,000 CPU-seconds for each run

other hand, advancements in hardware, such as post-processing [36], may help bridge the gap between this theoretical threshold and practical fabrication limits. Future research on optimization could explore assigning weights to objective function terms, leveraging machine learning to link objectives and yield, and implementing multilayered module assemblies. Furthermore, we note that even if the optimizer does not find the optimal allocation or if the fabricated chip does not fully meet all constraints, a best-effort solution still holds significant value. Specifically, techniques such as routing around dead qubits, quantum error correction schemes, and super-stabilizer methods [37, 38] can be employed to tolerate a small number of frequency collisions.

Future work may also involve developing application-specific designs [39, 40] rather than general-purpose quantum processors or optimizing total gate time that is also defined by qubit frequencies. The optimization techniques employed in this work may also be extended to

other SC circuit devices, such as fluxonium devices [41], remote CR coupling [42], and ZZ gates [43, 44]. One may also expect this optimizer to contribute to tunable couplers [45, 46] as a temporally local solver. Additionally, these methods could be applied to other quantum platforms with qubit-level control, including Rydberg atom tweezer arrays [47] or individually-controlled trapped ions [48–50].

ACKNOWLEDGMENTS

This work was supported by the U.S. Department of Energy, Office of Science, Office of Advanced Scientific Computing Research, under Contract No. DE-AC02-06CH11357 (Accelerated Research for Quantum Computing program, Fundamental Algorithmic Research for Quantum Utility project) and under Award Number DE-SC0021526.

-
- [1] F. Arute, K. Arya, R. Babbush, D. Bacon, J. C. Bardin, R. Barends, R. Biswas, S. Boixo, F. G. S. L. Brandao, D. A. Buell, B. Burkett, Y. Chen, Z. Chen, B. Chiaro, R. Collins, W. Courtney, A. Dunsworth, E. Farhi, B. Foxen, A. Fowler, C. Gidney, M. Giustina, R. Graff, K. Guerin, S. Habegger, M. P. Harrigan, M. J. Hartmann, A. Ho, M. Hoffmann, T. Huang, T. S. Humble, S. V. Isakov, E. Jeffrey, Z. Jiang, D. Kafri, K. Kechedzhi, J. Kelly, P. V. Klimov, S. Knysh, A. Korotkov, F. Kostritsa, D. Landhuis, M. Lindmark, E. Lucero, D. Lyakh, S. Mandrà, J. R. McClean, M. McEwen, A. Megrant, X. Mi, K. Michielsen, M. Mohseni, J. Mutus, O. Naaman, M. Neeley, C. Neill, M. Y. Niu, E. Ostby, A. Petukhov, J. C. Platt, C. Quintana, E. G. Rieffel, P. Roushan, N. C. Rubin, D. Sank, K. J. Satzinger, V. Smelyanskiy, K. J. Sung, M. D. Trevithick, A. Vainsencher, B. Villalonga, T. White, Z. J. Yao, P. Yeh, A. Zalcman, H. Neven, and J. M. Martinis, Quantum supremacy using a programmable superconducting processor, *Nature* **574**, 505 (2019).
- [2] Y. Kim, A. Eddins, S. Anand, K. X. Wei, E. van den Berg, S. Rosenblatt, H. Nayfeh, Y. Wu, M. Zaletel, K. Temme, and A. Kandala, Evidence for the utility of quantum computing before fault tolerance, *Nature* **618**, 500 (2023).
- [3] C. K. Andersen, A. Remm, S. Lazar, S. Krinner, N. Lacroix, G. J. Norris, M. Gabureac, C. Eichler, and A. Wallraff, Repeated quantum error detection in a surface code, *Nature Physics* **16**, 875 (2020).
- [4] N. Sundaresan, T. J. Yoder, Y. Kim, M. Li, E. H. Chen, G. Harper, T. Thorbeck, A. W. Cross, A. D. Córcoles, and M. Takita, Demonstrating multi-round subsystem quantum error correction using matching and maximum likelihood decoders, *Nature Communications* **14**, 2852 (2023).
- [5] M. P. Harrigan, K. J. Sung, M. Neeley, K. J. Satzinger, F. Arute, K. Arya, J. Atalaya, J. C. Bardin, R. Barends, S. Boixo, M. Broughton, B. B. Buckley, D. A. Buell, B. Burkett, N. Bushnell, Y. Chen, Z. Chen, B. Chiaro, R. Collins, W. Courtney, S. Demura, A. Dunsworth, D. Eppens, A. Fowler, B. Foxen, C. Gidney, M. Giustina, R. Graff, S. Habegger, A. Ho, S. Hong, T. Huang, L. B. Ioffe, S. V. Isakov, E. Jeffrey, Z. Jiang, C. Jones, D. Kafri, K. Kechedzhi, J. Kelly, S. Kim, P. V. Klimov, A. N. Korotkov, F. Kostritsa, D. Landhuis, P. Laptev, M. Lindmark, M. Leib, O. Martin, J. M. Martinis, J. R. McClean, M. McEwen, A. Megrant, X. Mi, M. Mohseni, W. Mroczkiewicz, J. Mutus, O. Naaman, C. Neill, F. Neukart, M. Y. Niu, T. E. O’Brien, B. O’Gorman, E. Ostby, A. Petukhov, H. Putterman, C. Quintana, P. Roushan, N. C. Rubin, D. Sank, A. Skolik, V. Smelyanskiy, D. Strain, M. Streif, M. Szalay, A. Vainsencher, T. White, Z. J. Yao, P. Yeh, A. Zalcman, L. Zhou, H. Neven, D. Bacon, E. Lucero, E. Farhi, and R. Babbush, Quantum approximate optimization of non-planar graph problems on a planar superconducting processor, *Nature Physics* **17**, 332 (2021).
- [6] F. B. Maciejewski, S. Hadfield, B. Hall, M. Hodson, M. Dupont, B. Evert, J. Sud, M. S. Alam, Z. Wang, S. Jeffrey, B. Sundar, P. A. Lott, S. Grabbe, E. G. Rieffel, M. J. Reagor, and D. Venturelli, Design and execution of quantum circuits using tens of superconducting qubits and thousands of gates for dense Ising optimization problems, *arXiv:2308.12423* (2023).
- [7] J. Zhang, R. Ferguson, S. Kühn, J. F. Haase, C. Wilson, K. Jansen, and C. A. Muschik, Simulating gauge theories with variational quantum eigensolvers in superconducting microwave cavities, *Quantum* **7**, 1148 (2023).
- [8] M. Dupont, B. Sundar, B. Evert, D. E. B. Neira, Z. Peng, S. Jeffrey, and M. J. Hodson, Quantum optimization for the maximum cut problem on a superconducting quantum computer, *arXiv:2404.17579* (2024).
- [9] T. Orell, A. A. Michailidis, M. Serbyn, and M. Silveri, Probing the many-body localization phase transition with superconducting circuits, *Physical Review B* **100**, 134504 (2019).

- [10] J. S. Hung, J. Busnaina, C. S. Chang, A. Vadiraj, I. Nsanzeze, E. Solano, H. Alaeian, E. Rico, and C. Wilson, Quantum simulation of the bosonic Creutz ladder with a parametric cavity, *Physical Review Letters* **127**, 100503 (2021).
- [11] H. Yu, Y. Zhao, and T.-C. Wei, Simulating large-size quantum spin chains on cloud-based superconducting quantum computers, *Physical Review Research* **5**, 013183 (2023).
- [12] M. Brink, J. M. Chow, J. Hertzberg, E. Magesan, and S. Rosenblatt, Device challenges for near term superconducting quantum processors: frequency collisions, in *International Electron Devices Meeting* (IEEE, 2018) pp. 6.1.1–6.1.3.
- [13] A. Morvan, L. Chen, J. M. Larson, D. I. Santiago, and I. Siddiqi, Optimizing frequency allocation for fixed-frequency superconducting quantum processors, *Physical Review Research* **4**, 023079 (2022).
- [14] P. Zhao, Mitigation of quantum crosstalk in cross-resonance-based qubit architectures, *Physical Review Applied* **20**, 054033 (2023).
- [15] A. G. Fowler, M. Mariantoni, J. M. Martinis, and A. N. Cleland, Surface codes: Towards practical large-scale quantum computation, *Physical Review A—Atomic, Molecular, and Optical Physics* **86**, 032324 (2012).
- [16] N. P. Breuckmann and J. N. Eberhardt, Quantum low-density parity-check codes, *PRX Quantum* **2**, 040101 (2021).
- [17] J.-P. Tillich and G. Zémor, Quantum LDPC codes with positive rate and minimum distance proportional to the square root of the blocklength, *IEEE Transactions on Information Theory* **60**, 1193 (2013).
- [18] S. Bravyi, A. W. Cross, J. M. Gambetta, D. Maslov, P. Rall, and T. J. Yoder, High-threshold and low-overhead fault-tolerant quantum memory, *Nature* **627**, 778 (2024).
- [19] C. Poole, T. Graham, M. Perlin, M. Otten, and M. Saffman, Architecture for fast implementation of qLDPC codes with optimized Rydberg gates, [arXiv:2404.18809](https://arxiv.org/abs/2404.18809) (2024).
- [20] P. Jurcevic, A. Javadi-Abhari, L. S. Bishop, I. Lauer, D. F. Bogorin, M. Brink, L. Capelluto, O. Günlük, T. Itoko, N. Kanazawa, A. Kandala, G. A. Keefe, K. Kruslich, W. Landers, E. P. Lewandowski, D. T. McClure, G. Nannicini, A. Narasgond, H. M. Nayfeh, E. Pritchett, M. B. Rothwell, S. Srinivasan, N. Sundaresan, C. Wang, K. X. Wei, C. J. Wood, J.-B. Yau, E. J. Zhang, O. E. Dial, J. M. Chow, and J. M. Gambetta, Demonstration of quantum volume 64 on a superconducting quantum computing system, *Quantum Science and Technology* **6**, 025020 (2021).
- [21] P. Gokhale, J. M. Baker, C. Duckering, N. C. Brown, K. R. Brown, and F. T. Chong, Asymptotic improvements to quantum circuits via qutrits, in *Proceedings of the 46th International Symposium on Computer Architecture* (2019) pp. 554–566.
- [22] C. Campbell, F. T. Chong, D. Dahl, P. Frederick, P. Goiporia, P. Gokhale, B. Hall, S. Issa, E. Jones, S. Lee, *et al.*, Superstaq: Deep optimization of quantum programs, in *International Conference on Quantum Computing and Engineering*, Vol. 1 (IEEE, 2023) pp. 1020–1032.
- [23] K. N. Smith, G. S. Ravi, J. M. Baker, and F. T. Chong, Scaling superconducting quantum computers with chiplet architectures, in *55th IEEE/ACM International Symposium on Microarchitecture* (IEEE, 2022) pp. 1092–1109.
- [24] J. Zhang, H. Wang, Q. Ding, J. Gu, R. Assouly, W. D. Oliver, S. Han, K. R. Brown, H. Li, and Y. Chen, Qplacer: Frequency-aware component placement for superconducting quantum computers, [arXiv:2401.17450](https://arxiv.org/abs/2401.17450) (2024).
- [25] K. Heya, M. Malekakhlagh, S. Merkel, N. Kanazawa, and E. Pritchett, Floquet analysis of frequency collisions, *Physical Review Applied* **21**, 024035 (2024).
- [26] W.-H. Lin, B. Tan, M. Y. Niu, J. Kimko, and J. Cong, Domain-specific quantum architecture optimization, *IEEE Journal on Emerging and Selected Topics in Circuits and Systems* **12**, 624 (2022).
- [27] T. Yang, W. Wang, L. Wang, B. Zhao, C. Liang, and Z. Shan, A superconducting quantum processor architecture design method for improving performance and reducing frequency collisions, *Results in Physics* **53**, 106944 (2023).
- [28] H. Kim, C. Jünger, A. Morvan, E. S. Barnard, W. P. Livingston, M. Altoé, Y. Kim, C. Song, L. Chen, J. M. Kreikebaum, D. F. Ogletree, D. I. Santiago, and I. Siddiqi, Effects of laser-annealing on fixed-frequency superconducting qubits, *Applied Physics Letters* **121** (2022).
- [29] E. J. Zhang, S. Srinivasan, N. Sundaresan, D. F. Bogorin, Y. Martin, J. B. Hertzberg, J. Timmerwilke, E. J. Pritchett, J.-B. Yau, C. Wang, W. Landers, E. P. Lewandowski, A. Narasgond, S. Rosenblatt, G. A. Keefe, I. Lauer, M. B. Rothwell, D. T. McClure, O. E. Dial, J. S. Orcutt, M. Brink, and J. M. Chow, High-performance superconducting quantum processors via laser annealing of transmon qubits, *Science Advances* **8**, eabi6690 (2022).
- [30] Y. Balaji, N. Acharya, R. Armstrong, K. G. Crawford, S. Danilin, T. Dixon, O. W. Kennedy, R. D. Pothuraju, K. Shahbazi, and C. D. Shelly, Electron-beam annealing of Josephson junctions for frequency tuning of quantum processors, [arXiv preprint arXiv:2402.17395](https://arxiv.org/abs/2402.17395) 10.48550/arXiv.2402.17395 (2024).
- [31] C. Berke, E. Varvelis, S. Trebst, A. Altland, and D. P. DiVincenzo, Transmon platform for quantum computing challenged by chaotic fluctuations, *Nature Communications* **13**, 2495 (2022).
- [32] A. Osman, J. Fernández-Pendás, C. Warren, S. Kosen, M. Scigliuzzo, A. Frisk Kockum, G. Tancredi, A. Fadavi Roudsari, and J. Bylander, Mitigation of frequency collisions in superconducting quantum processors, *Physical Review Research* **5**, 043001 (2023).
- [33] J. B. Hertzberg, E. J. Zhang, S. Rosenblatt, E. Magesan, J. A. Smolin, J.-B. Yau, V. P. Adiga, M. Sandberg, M. Brink, J. M. Chow, and J. S. Orcutt, Laser-annealing Josephson junctions for yielding scaled-up superconducting quantum processors, *npj Quantum Information* **7**, 129 (2021).
- [34] C. Rigetti and M. Devoret, Fully microwave-tunable universal gates in superconducting qubits with linear couplings and fixed transition frequencies, *Physical Review B—Condensed Matter and Materials Physics* **81**, 134507 (2010).
- [35] E. Magesan and J. M. Gambetta, Effective Hamiltonian models of the cross-resonance gate, *Physical Review A* **101**, 052308 (2020).
- [36] P. Gokhale, A. Javadi-Abhari, N. Earnest, Y. Shi, and F. T. Chong, Optimized quantum compilation for

- near-term algorithms with openpulse, in *53rd Annual IEEE/ACM International Symposium on Microarchitecture* (IEEE, 2020) pp. 186–200.
- [37] J. M. Auger, H. Anwar, M. Gimeno-Segovia, T. M. Stace, and D. E. Browne, Fault-tolerance thresholds for the surface code with fabrication errors, *Physical Review A* **96**, 042316 (2017).
- [38] S. F. Lin, J. Vízslai, K. N. Smith, G. S. Ravi, C. Yuan, F. T. Chong, and B. J. Brown, Codesign of quantum error-correcting codes and modular chiplets in the presence of defects, in *Proceedings of the 29th ACM International Conference on Architectural Support for Programming Languages and Operating Systems, Volume 2* (2024) pp. 216–231.
- [39] G. Li, Y. Ding, and Y. Xie, Towards efficient superconducting quantum processor architecture design, in *Proceedings of the Twenty-Fifth International Conference on Architectural Support for Programming Languages and Operating Systems* (2020) pp. 1031–1045.
- [40] Y. Ding, P. Gokhale, S. F. Lin, R. Rines, T. Propson, and F. T. Chong, Systematic crosstalk mitigation for superconducting qubits via frequency-aware compilation, in *2020 53rd Annual IEEE/ACM International Symposium on Microarchitecture (MICRO)* (IEEE, 2020) pp. 201–214.
- [41] E. Dogan, D. Rosenstock, L. Le Guevel, H. Xiong, R. A. Mencia, A. Somoroff, K. N. Nesterov, M. G. Vavilov, V. E. Manucharyan, and C. Wang, Two-fluxonium cross-resonance gate, *Physical Review Applied* **20**, 024011 (2023).
- [42] M. Ohfuchi and S. Sato, Remote cross-resonance gate between superconducting fixed-frequency qubits, *Quantum Science and Technology* **9**, 035014 (2024).
- [43] B. K. Mitchell, R. K. Naik, A. Morvan, A. Hashim, J. M. Kreikebaum, B. Marinelli, W. Lavrijsen, K. Nowrouzi, D. I. Santiago, and I. Siddiqi, Hardware-efficient microwave-activated tunable coupling between superconducting qubits, *Physical Review Letters* **127**, 200502 (2021).
- [44] Z. Huang, T. Kim, T. Roy, Y. Lu, A. Romanenko, S. Zhu, and A. Grassellino, Fast ZZ-free entangling gates for superconducting qubits assisted by a driven resonator, *Physical Review Applied* **22**, 034007 (2024).
- [45] L. Hour, S. Heng, S. Heng, M. Go, and Y. Han, Context-aware coupler reconfiguration for tunable coupler-based superconducting quantum computers, [arXiv:2401.03817](https://arxiv.org/abs/2401.03817) (2024).
- [46] P. V. Klimov, A. Bengtsson, C. Quintana, A. Bourassa, S. Hong, A. Dunsworth, K. J. Satzinger, W. P. Livingston, V. Sivak, M. Y. Niu, T. I. Andersen, Y. Zhang, D. Chik, Z. Chen, C. Neill, C. Erickson, A. Grajales Dau, A. Megrant, P. Roushan, A. N. Korotkov, J. Kelly, V. Smelyanskiy, Y. Chen, and H. Neven, Optimizing quantum gates towards the scale of logical qubits, *Nature Communications* **15**, 2442 (2024).
- [47] A. G. Radnaev, W. C. Chung, D. C. Cole, D. Mason, T. G. Ballance, M. J. Bedalov, D. A. Belknap, M. R. Berman, M. Blakely, I. L. Bloomfield, P. D. Buttler, C. Campbell, A. Chopinaud, E. Copenhaver, M. K. Dawes, S. Y. Eubanks, A. J. Friss, D. M. Garcia, J. Gilbert, M. Gillette, P. Goiporia, P. Gokhale, J. Goldwin, D. Goodwin, T. M. Graham, C. Guttormsson, G. T. Hickman, L. Hurlley, M. Iliev, E. B. Jones, R. A. Jones, K. W. Kuper, T. B. Lewis, M. T. Lichtman, F. Majdeteimouri, J. J. Mason, J. K. McMaster, J. A. Miles, P. T. Mitchell, J. D. Murphree, N. A. Neff-Mallon, T. Oh, V. Omole, C. P. Simon, N. Pederson, M. A. Perlin, A. Reiter, R. Rines, P. Romlow, A. M. Scott, D. Stiefvater, J. R. Tanner, A. K. Tucker, I. V. Vinogradov, M. L. Warter, M. Yeo, M. Saffman, and T. W. Noel, A universal neutral-atom quantum computer with individual optical addressing and non-destructive readout, [arXiv:2408.08288](https://arxiv.org/abs/2408.08288) (2024).
- [48] Y. Zhu, Z. Zhang, B. Sundar, A. M. Green, C. H. Alderete, N. H. Nguyen, K. R. Hazzard, and N. M. Linke, Multi-round QAOA and advanced mixers on a trapped-ion quantum computer, *Quantum Science and Technology* **8**, 015007 (2022).
- [49] L. Bond, L. Lenstra, R. Gerritsma, and A. Safavi-Naini, Effect of micromotion and local stress in quantum simulations with trapped ions in optical tweezers, *Physical Review A* **106**, 042612 (2022).
- [50] Y.-H. Hou, Y.-J. Yi, Y.-K. Wu, Y.-Y. Chen, L. Zhang, Y. Wang, Y.-L. Xu, C. Zhang, Q.-X. Mei, H.-X. Yang, *et al.*, Individually addressed entangling gates in a two-dimensional ion crystal, [arXiv preprint arXiv:2406.13999](https://arxiv.org/abs/2406.13999) [10.48550/arXiv.2406.1399](https://arxiv.org/abs/2406.13999) (2024).

The submitted manuscript has been created by UChicago Argonne, LLC, Operator of Argonne National Laboratory (“Argonne”). Argonne, a U.S. Department of Energy Office of Science laboratory, is operated under Contract No. DE-AC02-06CH11357. The U.S. Government retains for itself, and others acting on its behalf, a paid-up nonexclusive, irrevocable worldwide license in said article to reproduce, prepare derivative works, distribute copies to the public, and perform publicly and display publicly, by or on behalf of the Government. The Department of Energy will provide public access to these results of federally sponsored research in accordance with the DOE Public Access Plan <http://energy.gov/downloads/doe-public-access-plan>.